REPORT DOCUMENTATION PAGE

Form Approved OMB NO. 0704-0188

1. REPORT DATE (DD-MM-YYYY)	2. REPORT TYPE	3. DATES COVERED (From - To)
17-08-2010	Final Report	16-Nov-2009 - 16-Aug-2010

4. TITLE AND SUBTITLE
Self Regulating Fiber Fuel Cell

5a. CONTRACT NUMBER

5b. GRANT NUMBER
W911NF-10-C-0007

5c. PROGRAM ELEMENT NUMBER
9H20BA

6. AUTHORS
Steven J. Eickhoff

5d. PROJECT NUMBER

5e. TASK NUMBER

5f. WORK UNIT NUMBER

7. PERFORMING ORGANIZATION NAMES AND ADDRESSES
Honeywell Automation & Control Solutions
Honeywell Automation & Control Solutions
12001 State Hwy 55
Plymouth, MN 55441 -4799

8. PERFORMING ORGANIZATION REPORT NUMBER

9. SPONSORING/MONITORING AGENCY NAME(S) AND ADDRESS(ES)
U.S. Army Research Office
P.O. Box 12211
Research Triangle Park, NC 27709-2211

10. SPONSOR/MONITOR'S ACRONYM(S)
ARO

11. SPONSOR/MONITOR'S REPORT NUMBER(S)
57326-CH-DRP.1

12. DISTRIBUTION AVAILIBILITY STATEMENT
Approved for Public Release; Distribution Unlimited

13. SUPPLEMENTARY NOTES
The views, opinions and/or findings contained in this report are those of the author(s) and should not contrued as an official Department of the Army position, policy or decision, unless so designated by other documentation.

14. ABSTRACT
Advances in lithium primary battery technology, which serves as the gold standard power source for the dismounted soldier, have not kept pace with the ever increasing power and energy requirements of modern military electronic equipment. Fuel cells have long been touted as the solution to the dismounted soldier's power and energy problems, but until recently, have largely failed to live up to that promise. There is still a pressing need for better power sources at the Watt or sub-Watt level, especially in applications requiring non-traditional form factors (thin,

15. SUBJECT TERMS
Fuel Cells, Soldier Power, Micro Power, Fiber Fuel Cell

16. SECURITY CLASSIFICATION OF:			17. LIMITATION OF ABSTRACT	15. NUMBER OF PAGES	19a. NAME OF RESPONSIBLE PERSON
a. REPORT	b. ABSTRACT	c. THIS PAGE			Steven Eickhoff
UU	UU	UU	UU		19b. TELEPHONE NUMBER 763-954-2380

Standard Form 298 (Rev 8/98)
Prescribed by ANSI Std. Z39.18

Report Title

Self Regulating Fiber Fuel Cell

ABSTRACT

Advances in lithium primary battery technology, which serves as the gold standard power source for the dismounted soldier, have not kept pace with the ever increasing power and energy requirements of modern military electronic equipment. Fuel cells have long been touted as the solution to the dismounted soldier's power and energy problems, but until recently, have largely failed to live up to that promise. There is still a pressing need for better power sources at the Watt or sub-Watt level, especially in applications requiring non-traditional form factors (thin, prismatic) or those having special requirements like flexibility or conformability, where existing battery technology falls short. To address these needs, Honeywell has developed and demonstrated a revolutionary new power source in the form of a Self Regulating Fiber Fuel Cell, which utilizes a novel fuel chemistry, regulation mechanism and micro fabrication techniques to create a flexible, conformal power source with significantly better energy density and specific energy compared to state of the art lithium primary batteries. We have met all program objectives by demonstrating a 5mm diameter 50mm length fiber fuel cell with 93mW peak power, an energy density of 1027 Whr/liter and a specific energy of 1800Whr/kg, which corresponds to 7.4X and 15.4X the Solicore LiPo battery, respectively. We have demonstrated a fiber with bend radius of ~2-3mm which should enable weaving into a flexible and conformal mesh. We believe further performance improvements are possible through optimizing the fiber design.

List of papers submitted or published that acknowledge ARO support during this reporting period. List the papers, including journal references, in the following categories:

(a) Papers published in peer-reviewed journals (N/A for none)

Number of Papers published in peer-reviewed journals: 0.00

(b) Papers published in non-peer-reviewed journals or in conference proceedings (N/A for none)

Self-regulating fiber fuel cell
Proc. SPIE, Vol. 7683, 76830K (2010); doi:10.1117/12.853146

Number of Papers published in non peer-reviewed journals: 1.00

(c) Presentations

Number of Presentations: 0.00

Non Peer-Reviewed Conference Proceeding publications (other than abstracts):

Number of Non Peer-Reviewed Conference Proceeding publications (other than abstracts): 0

Peer-Reviewed Conference Proceeding publications (other than abstracts):

Number of Peer-Reviewed Conference Proceeding publications (other than abstracts): 0

(d) Manuscripts

Number of Manuscripts: 0.00

Patents Submitted

Patents Awarded

Awards

Graduate Students

NAME	PERCENT_SUPPORTED
FTE Equivalent:	
Total Number:	

Names of Post Doctorates

NAME	PERCENT_SUPPORTED
FTE Equivalent:	
Total Number:	

Names of Faculty Supported

NAME	PERCENT_SUPPORTED
FTE Equivalent:	
Total Number:	

Names of Under Graduate students supported

NAME	PERCENT_SUPPORTED
FTE Equivalent:	
Total Number:	

Student Metrics

This section only applies to graduating undergraduates supported by this agreement in this reporting period

The number of undergraduates funded by this agreement who graduated during this period:	0.00
The number of undergraduates funded by this agreement who graduated during this period with a degree in science, mathematics, engineering, or technology fields:.....	0.00
The number of undergraduates funded by your agreement who graduated during this period and will continue to pursue a graduate or Ph.D. degree in science, mathematics, engineering, or technology fields:.....	0.00
Number of graduating undergraduates who achieved a 3.5 GPA to 4.0 (4.0 max scale):	0.00
Number of graduating undergraduates funded by a DoD funded Center of Excellence grant for Education, Research and Engineering:	0.00
The number of undergraduates funded by your agreement who graduated during this period and intend to work for the Department of Defense	0.00
The number of undergraduates funded by your agreement who graduated during this period and will receive scholarships or fellowships for further studies in science, mathematics, engineering or technology fields:	0.00

Names of Personnel receiving masters degrees

NAME

Total Number:

Names of personnel receiving PHDs

NAME

Total Number:

Names of other research staff

NAME PERCENT_SUPPORTED

FTE Equivalent:

Total Number:

Sub Contractors (DD882)

Inventions (DD882)

Self-Regulating Fiber Fuel Cell

Contract Number W911NF-10-C-0007

Final Progress Report

Preparation Date: August 16, 2010

Prepared By:
Honeywell Laboratories
12001 State Highway 55
Plymouth, MN 55441-4799
Steven J. Eickhoff, Principal Investigator
Phone 763-954-2380 Fax 763-954-2380 Steven.Eickhoff@honeywell.com

For:
U.S Army Research Office
P.O. Box 12211
Research Triangle Park, NC 27709-2211

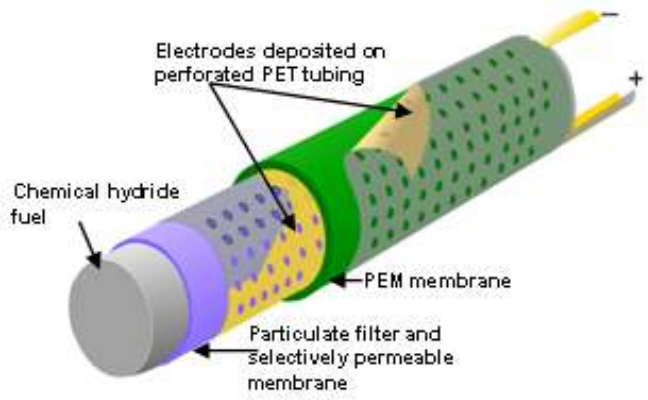

REPORT DOCUMENTATION PAGE

Form Approved
OMB No. 0704-0188

1. AGENCY USE ONLY (Leave blank)	2. REPORT DATE	3. REPORT TYPE AND DATES COVERED
	08-16-2010	Final Progress Report-November 2009 to August 2010

4. TITLE AND SUBTITLE	5. FUNDING NUMBERS
Self-Regulating Fiber Fuel Cell	W911NF-10-C-0007
6. AUTHOR(S)	
Steven J. Eickhoff	
7 PERFORMING ORGANIZATION NAME(S) AND ADDRESS(ES)	8. PERFORMING ORGANBIZATION REPORT NUMBER
Honeywell Laboratories 12001 State Highway 55 Plymouth, MN 55441-4799	
9. SPONSORING/MONITORING AGENCY NAME(S) AND ADDRESS(ES)	10. SPONSORING/MONITORING AGENCY REPORT NUMBER
U.S. Army Research Office P.O. Box 12211 Research Triangle Park, NC 27709-221	

11. SUPPLEMENTAL NOTES

The views, opinions and/or findings contained in this report of those of the author(s) and should not be construed as an official Department of the Army position, policy or decision, unless so designated by other documentation

12a. DISTRIBUTION/AVAILABILITY STATEMENT	12b. DISTRIBUTION CODE
Approved for public release; distribution unlimited	

13. ABSTRACT (Maximum 200 words

Honeywell Laboratories has designed, fabricated, and demonstrated prototype Self-Regulating Fiber Fuel Cells which utilizes a novel fuel chemistry, regulation mechanism, and micro fabrication techniques to create a flexible, conformal power source with substantially better energy density and specific energy compared to state of the art lithium primary batteries.

14. SUBJECT TERMS	15. NUMBER OF PAGES
	41
	16. PRICE CODE

17. SECURITY CLASSIFICATION	18. SECURITY CLASSIFICATION OF THIS PAGE	19. SECURITY CLASSIFICATION OF ABSTRACT	20. LIMITATION OF ABSTRACT
Unclassified	Unclassified	Unclassified	UL

NSN 7540-01-280-5500

Standard Form 298 (Rev. 2-89)
Prescribed by ANSI Std. Z39-18
298-102

Table of Contents

1.0 Executive Summary

Advances in lithium primary battery technology, which serves as the gold standard power source for the dismounted soldier, have not kept pace with the ever increasing power and energy requirements of modern military electronic equipment. Fuel cells have long been touted as the solution to the dismounted soldier's power and energy problems, but until recently, have largely failed to live up to that promise. There is still a pressing need for better power sources at the Watt or sub-Watt level, especially in applications requiring non-traditional form factors (thin, prismatic) or those having special requirements like flexibility or conformability, where existing battery technology falls short. To address these needs, Honeywell has developed and demonstrated a revolutionary new power source in the form of a Self Regulating Fiber Fuel Cell, which utilizes a novel fuel chemistry, regulation mechanism and micro fabrication techniques to create a flexible, conformal power source with significantly better energy density and specific energy compared to state of the art lithium primary batteries. We have met all program objectives by demonstrating a 5mm diameter 50mm length fiber fuel cell with 93mW peak power, an energy density of 1027 Whr/liter and a specific energy of 1800Whr/kg, which corresponds to 7.4X and 15.4X the Solicore LiPo battery, respectively. We have demonstrated a fiber with bend radius of ~2-3mm which should enable weaving into a flexible and conformal mesh. We believe further performance improvements are possible through optimizing the fiber design.

2.0 Statement of the Problem

Advances in lithium primary batteries, which serve as the gold standard power source for the dismounted soldier, have not kept pace with the ever increasing power and energy demands of modern military electronic equipment. In applications ranging from urban and tactical unmanned ground sensors to weapons systems, GPS, and night vision, current battery technology falls short in a number of areas including power, energy, weight, and form factor. Fuel cells have long been touted as the solution to the dismounted soldier's power and energy problems, and in recent years, significant progress has been made on fuel cells producing 10's of Watts and higher. Indeed, in DoD's Wearable Power Prize contest, several teams demonstrated 20 Watt fuel cell systems which successfully met the contest's power, energy, and weight objectives and in doing so have achieved superior specific energy to conventional lithium batteries [4]. Several of these fuel cells are currently under evaluation by the U.S Army for potential large scale use. Progress has also been made on fuel cells generating Watt or sub-Watt level power, but few have demonstrated superior performance to existing lithium primary batteries [5].

Clearly there is still a pressing need for better power sources at the Watt or sub-Watt level, particularly in applications requiring non-traditional form factors (thin, prismatic) or those having special requirements like flexibility or conformability, where existing battery technology falls short. Recently several companies have developed flexible/conformal lithium primary and rechargeable batteries in thin prismatic form factors. Flexibility/conformability has been achieved by adopting new and innovative fabrication and packaging methods, but with substantially reduced energy density (10-100X lower) vs. their conventional rigid counterparts. Lower energy density is driven primarily by dramatic reductions in the amount of energy containing active material as the size and cross section of the power source is reduced. While it is clearly desirable from an application standpoint to reduce the size of batteries and achieve flexibility and conformability, it is also important to maintain the high energy density of larger form factor batteries. The primary ways to accomplish this are to

1) Reduce packaging volume
2) Increase energy content of the active material
3) Increase conversion efficiency.

Honeywell's Self-Regulating Fiber Fuel Cell focuses on reducing packaging volume while increasing the energy density of the active material to deliver a power source with 7-10X the energy density and 10-15X the specific energy of state of the art flexible lithium polymer batteries. We accomplish this with a unique design utilizing a novel hydrogen generation process and regulation mechanism, coupled with micro-fabrication techniques.

State of the Art Thin and Flexible Power Sources

The state-of-the-art (SOA) in thin, flexible power sources are primarily of lithium polymer primary and lithium-ion polymer secondary batteries. In polymer batteries a lithium-salt electrolyte is contained in a polymer composite separator, which is laminated to the electrodes. This configuration eliminates the need for a heavy and rigid metal case to compress (and contain) the electrodes and electrolyte containing separator (as in conventional lithium primary and lithium-ion rechargeable batteries) and enables substantially thinner batteries capable of flexing without incurring damage. Table 1 summarizes the performance parameters and specifications of several thin and flexible batteries, a few thin and rigid batteries, a AA lithium primary battery, and two fuel cells. It also shows projections for the Honeywell fiber fuel cell concept in individual fiber and woven fiber mesh forms.

Table 1.Specifications of SOA thin and flexible batteries, AA lithium primary battery, fuel cells, and Honeywell's Fiber Fuel Cell

Device	Description	Manufacturer	Size (L X W X H) in mm:	Capacity (mWhr)	Energy density (mWhr/cc)	Specific Energy (mWhr/g)
Enerchip CBC050	Rigid thin-film Li-ion in SMT package	Cymbet	8 X 8 X 1	0.2	3	<1.5
MEC101-7P	Flexible thin-film Li-ion	Infinite Power Solutions	30 X 30 X 1	3	3.3	6.7
ORLI 0.5.CL	Rigid thin-film Li-ion	Oak Ridge Micro Energy	13 X 13 X 0.62	0.17	1.6	0.85
STD-2	Flexible thin-film alkaline MnO2	Power Paper	55 X 55 X 0.7	45	21	<21
Flexion SF-4823	Flexible Li-poly	Solicore	48.75 X 23 X 0.45	70	139	116.7
AA LS14500	AA lithium-thionyl chloride primary	Saft	Diameter: 14.65 Height: 50.3	5000	625	308.6
MiniPak	Rigid solid state hydrogen fuel cell	Horizon	104 X 68 X 25	12000	68.2	77.4
24/7 Extreme	Rigid liquid hydrogen fuel cell	Medis	68 X 97 X 57	20000	53.2	108.1
Fiber Fuel Cell	Flexible Individual fiber	Honeywell	Diameter: 1 Height: 50	71.7	1825	1841
Fiber fuel cell mesh	Flexible Woven fiber mesh	Honeywell	50 X 50 X 2	5363	1073	1841

Presently, the Flexion SF-4823 has the highest energy density of any commercially available thin and flexible power source. The SF-4832 is a lithium polymer primary battery manufactured by Solicore. It has dimensions 48.75 mm X 23 mm X 0.45 mm, a total energy capacity of 70mWhr, and energy density of 139mWhr/cc. By comparison, our models project for an individual fiber fuel cell of 5 cm length and 1mm diameter an energy density of 1825mWhr/cc, or >13X greater than the Flexion SF-4823. Similarly, projections for a woven mesh of fiber fuel cells with dimensions 50 mm X 50 mm X 2 mm yield an energy density of 1073mWhr/cc, or 7.7X greater than the Flexion SF-4823. The prospective energy density (and subsequently run time) improvement of the fiber fuel cell and fiber fuel cell mesh vs. SOA represent a truly revolutionary increase in capability.

3.0 Design, Operation, and Performance Projections

The fiber fuel cell as envisioned in Figure 1 is a small diameter (<1mm) flexible, high-aspect ratio cylinder, similar to the thread of a fabric. At the core of the fiber is porous lithium aluminum hydride (LiAlH4), which comprises the majority (>70%) of the fiber volume. Pores in the LiAlH4 fuel allow water vapor and hydrogen to freely diffuse in and out, respectively, and to provide expansion room for the LiALH4 reaction

products, which are more massive and less dense than the LiAlH4. Surrounding the core is a selectively permeable membrane (SPM) which allows hydrogen and water vapor to permeate freely but prevents liquids from entering or fuel particles from escaping. The SPM permeability is selected based on desired power output and environmental operating range. Surrounding the SPM is the anode electrode, together forming a perforated, and thin-wall PET shrink tube substrate with a gold electrode plated on the surface. The gold electrode serves as anode current collector for the fuel cell. The perforated PET tube containing the LiAlH4 fuel while allows gases to diffuse through. The membrane electrode assembly (MEA) surrounds the anode electrode, and comprises a proton exchange membrane with catalyst coating. The MEA is the active portion of the fuel cell which converts hydrogen from the anode and oxygen from the cathode to electricity and water. The outer-most layer of the fiber, and surrounding the MEA, is the cathode electrode. Similar to the anode electrode, it is a perforated thin-wall PET shrink tube with a gold electrode on the surface. On the cathode electrode, gold is plated on the inner surface of the tube and makes electrical contact to the MEA cathode. The cathode electrode compresses the MEA against the anode electrode, and these three layers together form the fuel cell. Output electrodes (shown in the upper right of figure 1) are extensions of the anode and cathode electrodes. The small fiber diameter and thin, flexible polymer construction enable flexibility and the potential to weave the fibers into a "power cloth."

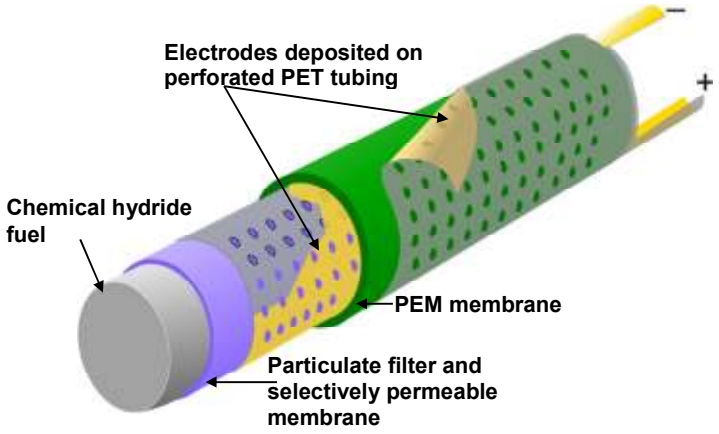

Figure 1. Fiber fuel cell schematic

Principles of Operation

The fiber fuel cell comprises a hydrogen-air proton exchange membrane (PEM) fuel cell coupled to a self regulating hydrogen generator. Hydrogen produced by the hydrogen generator and oxygen from ambient air react in the fuel cell, generating electrical energy and water vapor by the following reactions:

$$\text{Fuel cell anode reaction: } 4H_2 \rightarrow 8H^+ + 8e^-$$

$$\text{Fuel cell cathode reaction: } 2O_2 + 8H^+ + 8e^- \rightarrow 4H_2O + Energy$$

$$\text{Overall reaction: } 4H_2 + 2O_2 \rightarrow 4H_2O + Energy \quad (1)$$

Water vapor generated at the fuel cell cathode permeates through the PEM in the fuel cell back into the power generator and reacts with LiAlH4 to generate hydrogen by the following reaction:

$$LiAlH_4 + 4H_2O \rightarrow 4H_2 + Solids \quad (2)$$

The water vapor permeates the PEM due to a large concentration gradient between the fuel cell cathode where the water vapor is produced, and the LiAlH4 core, which is very dry due to the reactivity of LiAlH4. Adding reactions (1) and (2) gives the net reaction (3) of the power generator as

$$LiAlH_4 + 2O_2 \rightarrow 4H_2 + solids \quad (3)$$

The net reaction is water neutral, generates no gas phase byproducts, and consumes only oxygen from the air. The reaction is thus "water-less" and does not require onboard water storage or management. This substantially simplifies the construction and improves the energy density and specific energy of the fiber fuel cell relative to other hydride approaches in which the water is stored and managed onboard.

The electrical work for hydrogen converted into electrical energy in a hydrogen-oxygen PEM fuel cell operating at a cell potential of 0.6 Volts (~50% chemical to electrical conversion efficiency) can be calculated using equation (4)

$$W = nNFE \quad (4)$$

where *W* is the electrical work in Joules, n is the number of electrons generated per molecule of hydrogen, *N* is the number of molecules of hydrogen, *F* is Faraday's constant, and *E* is the cell potential. The resulting electrical work per mole of LiAlH4 is 46.3 kJ, or 128.7 Whr. The energy density (Whr/liter) of LiAlH4 can be calculated using equation (5)

$$ED = W\frac{\rho}{m} \quad (5)$$

where *ED* is the energy density in Whr/liter, W is the electrical work, ρ is the density and *m* is the molecular mass of LiAlH4. Assuming 18% porous LiAlH4 with a density of 0.75 g/cc (crystal density is 0.917 g/cc) the energy density is 2540 Whr/liter. Similarly, the specific energy can be calculated using equation (6)

$$SE = \frac{W}{m} \quad (6)$$

where *SE* is the specific energy in Whr/kg, W is the electrical work, and m is the molecular mass of LiAlH4. The specific energy is 3380 Whr/kg. These fuel-only energy density and specific energy numbers are 2.3X and 5.7X the theoretical values for lithium thionyl chloride respectively (1100 Whr/liter and 590 Whr/kg), which has the highest energy density and specific energy of any commercially available lithium battery chemistry [1].

Due to the large water concentration gradient between the fuel cell cathode and LiAlH4 fuel in the hydrogen generator, water vapor from the ambient environment will permeate the PEM in the fuel cell and continue to generate hydrogen even when there is no electrical load on the fuel cell. Without a regulation mechanism to stop the water permeation (or eliminate excess hydrogen) hydrogen pressure inside the fiber would rise, eventually causing the fiber to burst. In previous programs Honeywell has developed larger form factor fuel cells which utilize a passive pneumatic valve to regulate the hydrogen generation rate by controlling water diffusion from the fuel cells to the chemical hydride fuel. The valve enables the fuel cell to adapt to changes in electrical load by varying the hydrogen generation rate, and even stop generating hydrogen when the load is removed. Figure 2 shows a schematic of a fuel cell with a pneumatic valve.

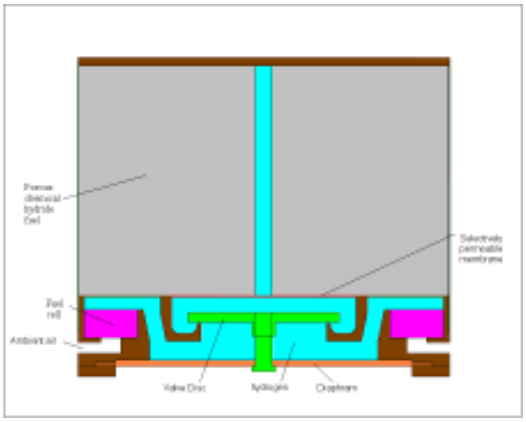

Figure 2. Schematic of a fuel cell with a pneumatic valve. The diaphragm flexes based on pressure difference across it, changing the conductance of the path between the fuel cells and chemical hydride fuel source, thus regulating the hydrogen generation rate.

While this valve architecture is suitable for larger fuel cells, it becomes increasingly difficult to implement as the size is reduced. At the mm scale this valve architecture is difficult and expensive to build, limits power output, and dominates the weight and volume of the fuel cell, resulting in poor energy density and specific energy. Small scale power sources thus require a different regulation mechanism to achieve high performance.

In the fiber fuel cell, an alternative regulation mechanism is utilized, wherein rising hydrogen pressure not only acts as a feedback mechanism for lowering the hydrogen generation rate by reducing the water permeation rate, but also causes increased hydrogen permeation losses through the PEM to ambient. Both mechanisms work in concert to stabilize the pressure and allow the fiber fuel cell to operate without a valve, the details of which are discussed below.

The hydrogen permeation rate through the PEM can be calculated using equation (7)

$$J_{H_2} = P_M \frac{A\Delta P}{t} \quad (7)$$

where J_{H_2} is the hydrogen permeation rate in mol/sec, P_M is the membrane permeability, A is the membrane area, ΔP is the hydrogen pressure difference across the membrane, and t is the membrane thickness. The membrane permeability can be expressed as the product of solubility and diffusivity as in equation (8)

$$P_M = SD \quad (8)$$

Where S is the solubility and D is the diffusivity. Solubility and diffusivity data vs. pressure for hydrogen in Nafion is not available in the literature, however permeability data is available and is relatively independent of pressure in the pressure range of interest (0 to 10 atmospheres) [2]. The hydrogen permeation rate is thus directly proportional to the hydrogen pressure difference across the PEM.

The water vapor permeability rate in Nafion membranes in the presence of an adverse hydrogen pressure gradient (between fuel cell anode and cathode) is not available in the published literature. We have determined the permeability by measuring the relative humidity vs. time in a test cell in which the anode and cathode of the cell are initially fixed at 25% RH and 80% RH, respectively, for a range pressures at the anode, with atmospheric pressure at the cathode. This data is presented in figure 3, and shows a reduction in the rate of relative humidity rise (permeation rate) as the anode pressure is increased.

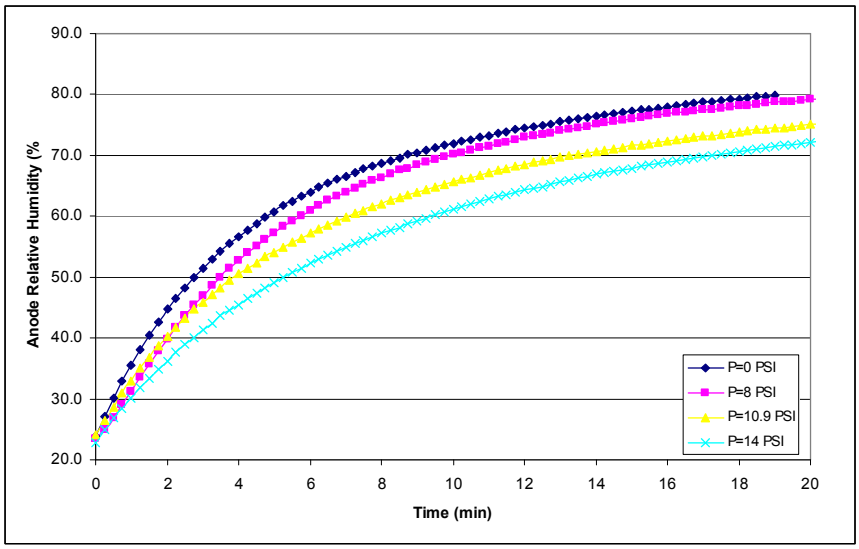

Figure 3. Relative humidity vs. time at the anode of a fuel cell for anode hydrogen pressures ranging from 0 to 14 PSI gauge

The effect of anode pressure on water vapor permeability is seen more clearly in figure 4, in which the rate of humidity increase vs. anode pressure is plotted.

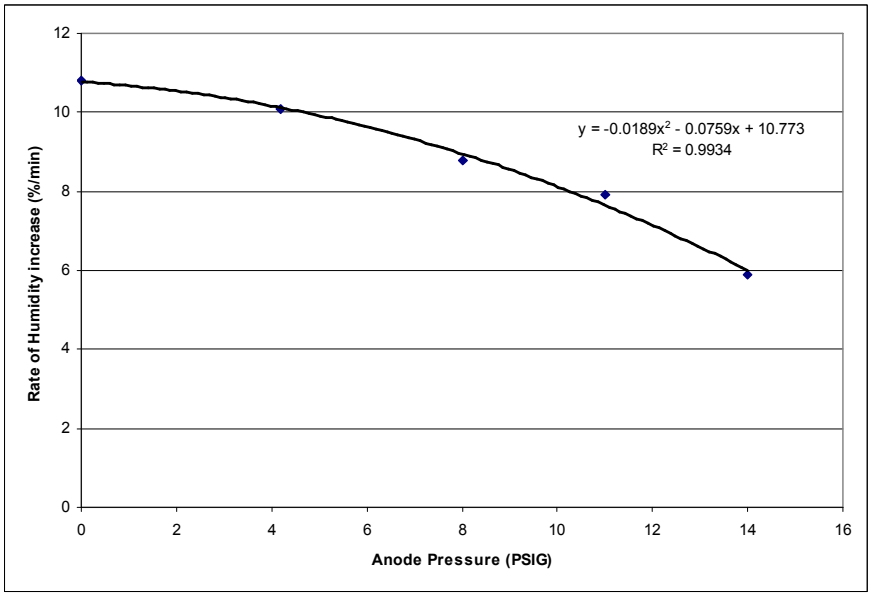

Figure 4. Rate of humidity increase vs. anode pressure in the anode of a fuel cell.

The rate of humidity rise shown in figure 4, which is proportional to the water vapor permeability, is reduced by 47% as the anode pressure is doubled. Based on quadratic least squares fit of the data shown in figure 4, the water vapor permeation rate is expressed in equation (9) as

$$J_{H_2O} = -k_1 P^2 - k_2 P + k_3 \quad (9)$$

where J_{H_2O} is the water vapor permeation rate, k_1, k_2, k_3 are known constants, and P is the hydrogen pressure. The rate of change of hydrogen pressure ($\frac{dP}{dt}$) in the fiber fuel cell is equal to the hydrogen generation rate minus the hydrogen consumption rate minus the hydrogen permeation rate and is expressed in equation (10) as

$$\frac{dP}{dt} = k_1 J_{H_2O} - k_2 I - k_3 P \quad (10)$$

where *P* is the hydrogen pressure, k_1, k_2, k_3 are known constants (different from above), J_{H_2O} is the water permeation rate, I is the current. Substituting equation (9) into equation (10), assuming zero current (worst case for maximum pressure), and setting the rate of change of pressure with time to zero (pressure stability) gives equation (11)

$$k_1 P^2 + k_2 P = 0 \quad (11)$$

Equation (10) is solved to give the maximum operating pressure for the fiber fuel cell. Based on the desired operating temperature and humidity range, as well as the design parameters for the fiber, the maximum operating pressure is projected to be <50 psi, which should result in reasonable self discharge rates and won't require thick and heavy tubing to contain.

Performance Projections

Performance projections for three fiber fuel cell configurations spanning a range of power output from 15mW to 20W from are shown in Table 2. The three configurations demonstrate the scalability of the fiber concept. The first configuration is an individual fiber of 1mm diameter and 50 mm length. The second configuration is a 50 mm X 50 mm X 2 mm woven fiber mesh. The mesh is composed of 75 individual 1mm diameter fibers woven together to form a flexible "power cloth." The fibers that make up the cloth may be connected electrically in any desired series/parallel configuration to deliver an output voltage under load in the range of 0.6-45V. The third configuration is a much larger power source designed to meet the 20 Watt average power, 96 hour mission duration objectives of the DOE Wearable Power Program. It is a 37 cm X 37 cm X 1 cm woven mesh composed of 111 individual 5mm diameter fibers. This configuration can deliver an output voltage under load in the range of 0.6-66.6 V. The energy density and specific energy of the 5mm fiber mesh is substantially higher than the 1mm fiber mesh due to a higher fuel to packaging mass and volume ratio. This results in higher energy density and specific energy for the large fiber mesh.

Table 2. Performance projections for three fiber fuel cell configurations

Config	Size	Capacity	Mass	Volume	Energy Density	Specific Energy	Power	Power Density	Specific Power
	(L X W X H) in cm	(mWhr)	(g)	(cc)	(mWhr/cc)	(mWhr/g)	(mW)	mW/cc	(mW/g)
Individual fiber	Diameter: 0.1 Length: 5	71.7	0.04	0.039	1825	1793	15	385	375
Small fiber mesh	5 X 5 X 0.2	5364	2.9	5	1073	1850	1200	240	414
Large fiber mesh	37 X 37 X 1	1.92E+06	645	1369	1404	2978	20000	14.6	31.1

The projected performance of all three fiber configurations is substantially better than SOA batteries and fuel cells. The large fiber mesh, for example, is projected to achieve 1404 Whr/liter and 2978Whr/kg, or 6.25X and 14.9X the BA5390 respectively, which is one of the most widely used military lithium primary

batteries. Similarly, the large fiber mesh also outperforms the winning entry of the DOE Wearable Power Program, a fuel cell system which achieved ~510 Whr/kg.

4.0 Summary of Results

Honeywell has successfully developed and demonstrated fiber fuel cell prototypes which achieve the program objectives relative to power, energy density, specific energy, and has experimentally validated the "self-regulation" mechanism. The following sections cover prototype fabrication, assembly, testing, and demonstrated performance.

Prototype Fabrication, Assembly, and Testing

Our initial approach to fabricating the fiber electrodes (described in section 3.0) was to use an electro-less plating process to deposit a copper seed layer on thin-walled PET shrink tubing, followed by an electroplating process to deposit the gold contact. We conducted a range of plating experiments (described in detail in appendix 1) but were unable to achieve adequate seed layer adhesion to the PET substrate, resulting in a poor quality contact. Based on an extensive literature survey we determined that poor adhesion resulted from high residual stress inherent in shrink tubing. We believe that with additional experiments the plating process could be optimized to produce a seed layer with better adhesion, however, in the interest of achieving the program objectives in the short period of performance of the program, we modified our electrode fabrication process to a lower-risk gold-on-Kapton approach with which we have extensive experience.

Our second approach to fabricating the fiber electrodes utilized an evaporated gold-on-Kapton process which we developed in a previous program. In this process the electrodes are created by patterning gold on a thin, planar Kapton substrate using a shadow mask. A laser cut process was used to perforate and release the electrodes from the Kapton substrate. A photo of the shadow mask is presented in figure 5, while a photo of a released electrode is presented in figure 7 a).

Figure 5. Photo of shadow mask used for patterning metal on the fiber electrodes

The remaining components (adhesives, MEA, selectively permeable membranes) were cut from sheet stock with a laser. Fuel pellets of the desired particle size, distribution, and porosity are pressed using a custom-fabricated die. A photo of the die is presented in figure 6.

Figure 6. Photo of die used for pressing LiAlH4 fuel pellets

Fibers are assembled in planar form, wrapped around a cylindrical mandrel, and compressed in place with a perforated PET shrink tube. Photos of a fiber in various stages of assembly are presented in figure 7. The assembly process moves sequentially from the anode electrode on the left, to a completed fiber on the right. The assembly process is as follows:

a) Placement of anode electrode in assembly fixture
b) Apply anode double sided adhesive to anode electrode
c) Apply MEA to adhesive
d) Apply cathode double sided adhesive to MEA
e) Apply cathode electrode to cathode double sided adhesive
f) Apply selectively permeable membrane to anode and cathode electrodes, compress using hydraulic press
g) Wrap fiber on test mandrel, compress in place with perforated PET shrink tubing and anneal process

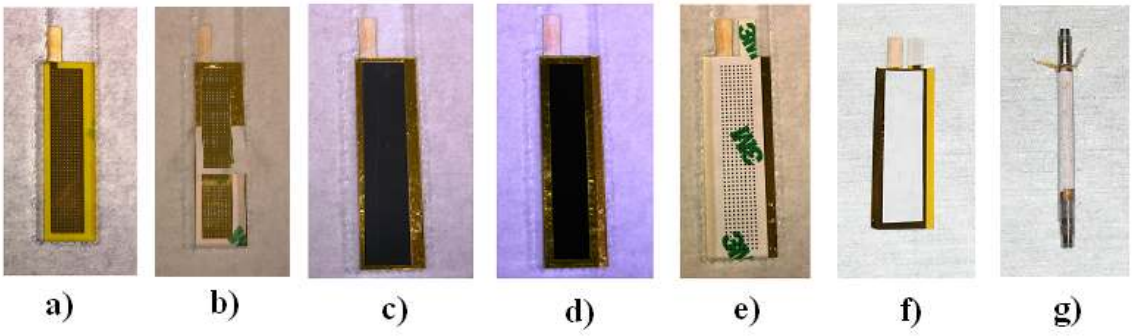

Figure 7. Planar fiber assembly process shown sequentially from left to right.

Following step g) the completed fiber is tested with hydrogen gas, and polarization data is recorded. The hydrogen leak rate is also determined by pressurizing the cell with hydrogen and monitoring pressure decay vs. time. The fiber is then removed from the mandrel and filled with LiAlH4 fuel pellets. The fiber mass, fiber volume, fuel loading, bend radius are measured. The fiber is then placed on the fiber holder, a close-up photo of which is shown in figure 8. A photo of the complete fiber test fixture is shown in figure 9.

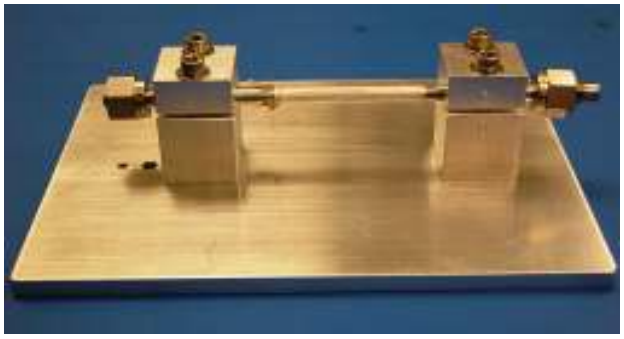

Figure 8. Photo of fiber fuel cell in the fiber holder

Figure 9. Photo of test fixture comprising the fiber holder, cables leading to a MACOR 4300 programmable electronic load, tubing leading to gas (nitrogen and hydrogen) handling equipment, a suite of sensors including pressure, temperature, and humidity. The beaker of water in the upper left enables visual detection of flow during flushing operations, and prevents air from diffusing back into the fiber.

The electrical performance (power and energy) with LiAlH4 fuel, as well as validation of self regulation is tested with the following procedure:

1) Flush fiber with nitrogen
2) Flush fiber with hydrogen
3) Discharge fiber at 0.6V constant potential using electronic load
4) Monitor pressure, current, voltage, temp, RH, until current drops below 1mA
5) Validate self regulation by periodically interrupting discharge and allowing pressure to stabilize

Test results and discussion are presented in the following section.

Test Results

Seven fiber fuel cell prototypes were fabricated and tested during the program; their specifications and performance relative to program goals are presented in table 3. All performance goals were met by at least one fiber, and fiber 7 met all goals. Fibers 1-4 were tested with hydrogen fuel to focus on improving fuel cell electrical performance, eliminate gas leaks, and to develop and refine assembly and test procedures. Fibers 5-7 were tested with LiAlH4 fuel to determine energy density and specific energy and to validate

self regulation. Select data from several fibers are presented below to demonstrate different aspects of fiber performance.

Table 3. Summary of fiber fuel cell performance against project goals

	Goal	Fiber 1	Fiber 2	Fiber 3	Fiber 4	Fiber 5	Fiber 6	Fiber 7
Mass (g)	<0.667	0.198	0.199	0.198	0.199	0.499	0.507	0.549
Volume (cc)	1	1	1	1	1	1	1	1
OCV (Volts)	>0.9	0.66	0.93	0.91	0.91	0.83	0.91	0.95
Peak Power (mW)	70	49	84	80	89	54	93	91
Energy (Whr)	>1	NA	NA	NA	NA	0.428	0.74	0.988
Energy Density (Whr/liter):	>1000	NA	NA	NA	NA	445	769	1027
Specific Energy (Whr/kg):	>1500	NA	NA	NA	NA	858	1460	1800

Fiber 1 was tested with hydrogen fuel on a supporting mandrel (see figure 7 g). Polarization data for fiber 1 is presented in figure 10. The fiber contains a single fuel cell, so we expect an open circuit voltage (OCV) of around 0.9-0.95 volts, and peak power between 70-100mW. The OCV for fiber 1 was 0.66V, and the peak power was 49mW. The low OCV and power indicate a low resistance electrical short inside the cell. Fiber 1 also had a high hydrogen leak rate, (>1A current equivalent) which is suggestive of a poor seal between the adhesives and MEA. A tear-down analysis of the cell confirmed an electrical short due to poor alignment between the electrodes and adhesive, which also resulted in a poor seal between the adhesive and MEA and cause the hydrogen leak. To address these problems fixtures for aligning the electrodes and adhesives during assembly were developed and employed in all subsequent prototype builds.

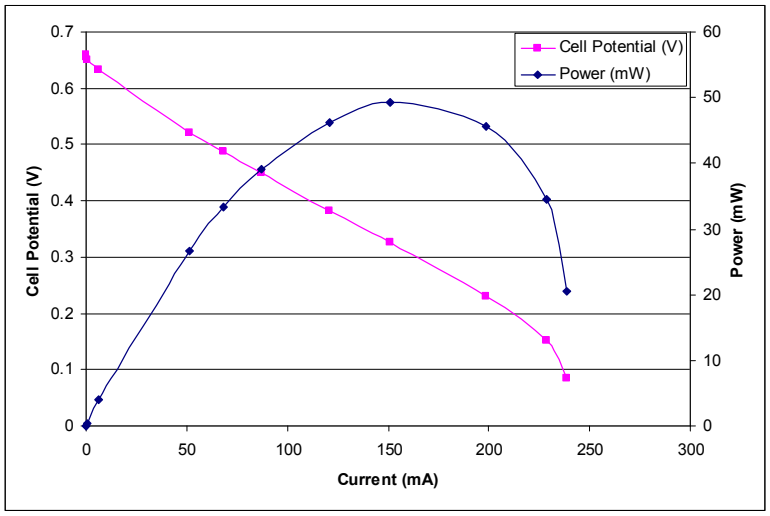

Figure 10. Polarization data for fiber 1

Fiber 2 was tested with hydrogen fuel on a supporting mandrel. Polarization data for fiber 2 is presented in figure 11 a). The problems with low OVC and power were eliminated, and fiber 2 met the program OCV and power objectives with a 0.93V OCV and 84mW peak power. The stability and durability of the fiber was tested via a constant potential test with hydrogen fuel, and is presented in figure 11 b). Power output was stable and increasing throughout the test as the proton exchange membrane "broke in" and its ionic conductivity increased over time. The hydrogen leak rate was improved versus fiber 1 (775mA current equivalent) but was still higher than expected. An epoxy adhesive seal at the ends of the fiber where the fiber sealed to the test fixture was added in fiber 3 to reduce the leak rate.

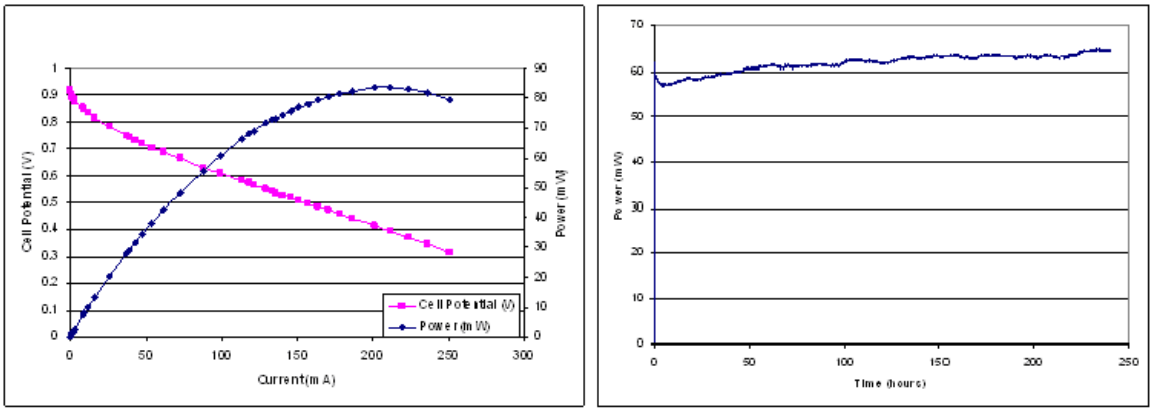

a) b)

Figure 11. Polarization data (a) and constant potential discharge data (b) for fiber 2

Fibers 3 and 4 were tested with hydrogen fuel without a supporting mandrel. Polarization and power data were consistent with fiber 2 and are not shown. The leak rate of fiber 4 was improved slightly to 549mA current equivalent with the addition of epoxy seals at the ends of the fibers. Leak rate data for fiber 4 is presented in figure 12.

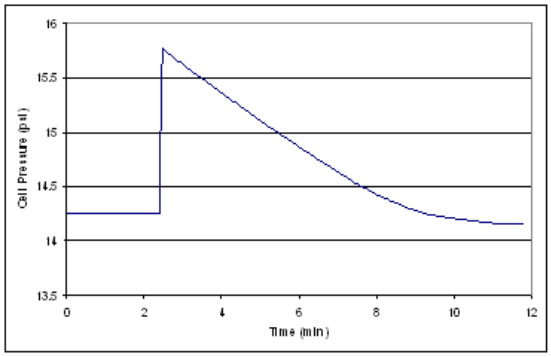

a)

Ambient Temp ©:	2.20E+01
Ambient Pressure (psi):	1.42E+01
Leak rate (psi/sec):	2.45E-01
Fixture volume (cc):	3.14E+00
Fiber Volume (cc):	1.00E+00
Leak rate (mol/sec):	2.84E-06
Current equivalent leak rate (mA):	5.49E+02

b)

Figure 12. Pressure decay data (a) and calculation (b) of the leak rate of fiber 4

Fiber 5 was the first prototype tested with LiAlH4 fuel. OCV and power were 0.83V and 54mW, which was slightly lower than expected due to a defect in the adhesive which resulted in a low resistance electrical short. Extracted energy was 0.428Whr, which equates to 445 Whr/liter and 858Whr/kg. Fuel utilization was a low 42%, which is reasonable given the high hydrogen leak rate of 560mA current equivalent, and the low resistance electrical short. Discharge data (power and energy) for fiber 5 is presented in figure 13.

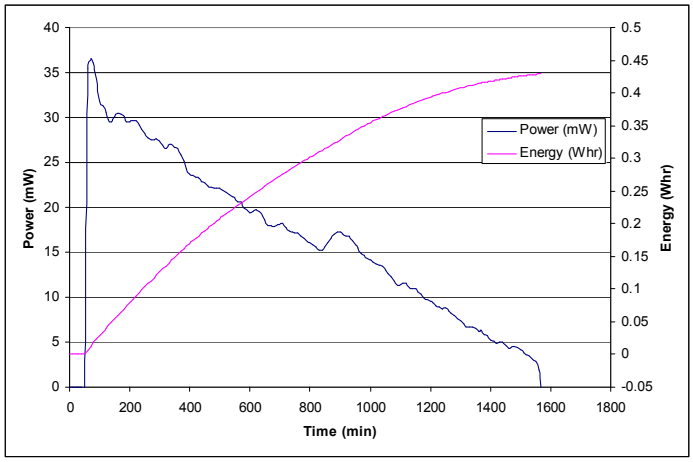

Figure 13. Power and energy data for fiber 5.

Fiber 6 was tested with LiAlH4 fuel. The fiber was compressed in planar form in a hydraulic press in attempt to improve the gas seals and reduce leak rates. OCV and peak power were 0.91V and 93mW, indicating a properly functioning fuel cell. The leak rate was 4.7mA current equivalent, >100X reduction vs. previous prototypes and an indication that the press process was successful in reducing leak rates. Extracted energy was 0.74Whr, which equates to 769Whr/liter and 1460Whr/kg. Fuel utilization was improved to 73%, which is consistent with a properly functioning fuel cell and lower leak rate. Discharge data (power and energy) for fiber 6 is presented in figure 14. The noise in the power data beginning at around 2400 min is caused by the electronic load as it reached its lower limit for current control.

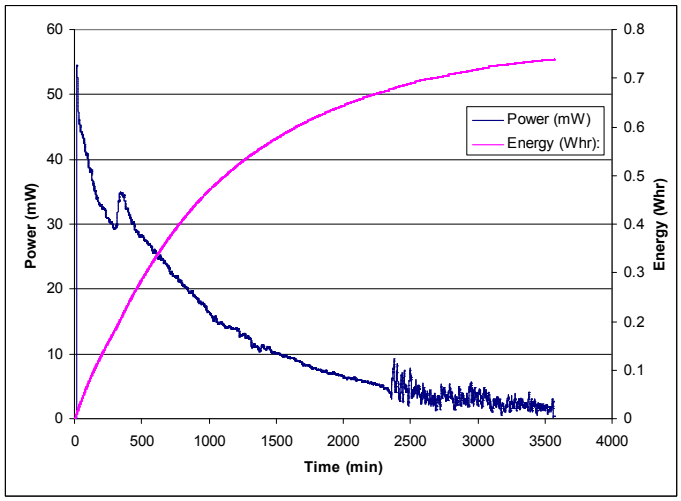

Figure 14. Power and energy data for fiber 6.

Fiber 7 represents the culmination of work on the program, and incorporates the improvements made in fibers 1-6. It was tested with LiAlH4 fuel, but at a 15% higher loading. OCV and peak power were 0.95V and 91mW, indicating a properly functioning fuel cell. The leak rate was a low 4.9mA current equivalent. Extracted energy was 0.988Whr, which equates to an energy density of 1027 Whr/liter, and a specific energy of 1800Whr/kg. By comparison, the energy density and specific energy of fiber 7 are 7.4X and 15.4X greater, respectively than the Solicore LiPo battery, representing a truly revolutionary performance improvement. Fuel utilization was 83.3%, leaving additional margin for improvement in future designs, via

optimization of fuel porosity and particle size, and further reduction in leak rate. Discharge data (power and energy) for fiber 7 is presented in figure 15. The noise in the power data beginning at around 3200 min is caused by the electronic load as it reached its lower limit for current control.

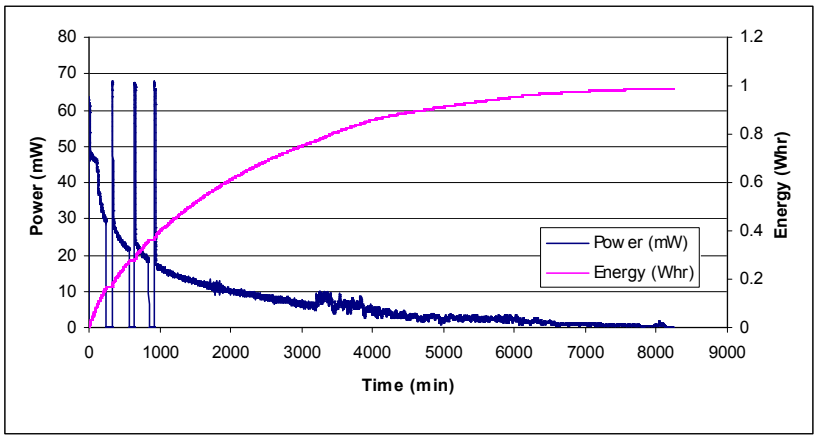

Figure 15. Power and energy data for fiber 7.

The three power transients in the first 1000 minutes resulted from temporary removal of the electronic load intended to demonstrate self regulation. Figure 16 shows the first 1000 minutes of the test in more detail, in a plot of power and cell pressure vs. time.

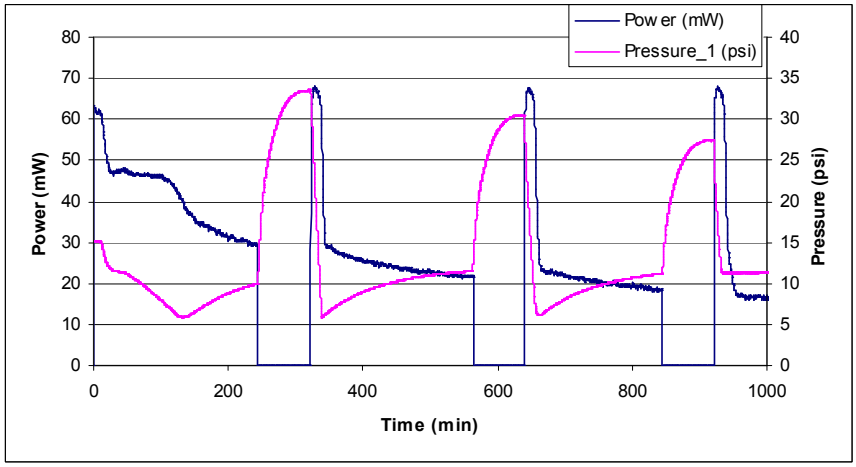

Figure 16. First 1000 minutes of fiber 7 discharge. Electronic load is removed for a period of time, cell pressure rises and stabilizes. Electronic load is reapplied, causing power transient until pressure drops back to equilibrium value. The fiber was tested under 0.6V constant potential, thus the power is lower than the peak power (which occurs at ~0.4V)

The pressure rises following removal of the electronic load, but stabilizes at a higher value after a period of time. Following pressure stabilization, the electronic load is reapplied and the pressure drops to its equilibrium value. The power increases during this time due to higher hydrogen pressure. The stabilization pressure for each subsequent transient is lower than the last, which is expected due to rising internal mass transfer resistance as the LiAlH4 fuel is consumed and reaction products form. For the design and ambient conditions of this test we predict a mid-discharge stabilization pressure of 32 psi, which is validated by the experimental data.

The bend radius of fiber 7 was tested by wrapping it around mandrels of decreasing diameter until we felt it would bend no more without kinking or breaking. Using this qualitative measure we found that the fiber has a bend radius of ~2-3mm, which should be sufficient for weaving given the 2.5mm radius (5mm diameter) of the fiber. We expect smaller bend radii for smaller diameter fibers (on the order of the fiber radius), which should make it possible to weave the fibers into a flexible and conformal mesh. Increased flexibility can be had at the price of energy, thus a more flexible fiber mesh would have a slightly lower energy density and specific energy.

5.0 Conclusions

Honeywell has designed, fabricated, and demonstrated prototype Self-Regulating Fiber Fuel Cells which meet or exceed the program goals and successfully validate the self regulating concept. We have achieved an energy density of 1027 Whr/liter and a specific energy of 1800Whr/kg, or 7.4X and 15.4X the Solicore LiPo battery, respectively. We have demonstrated a fiber bend radius of ~2-3mm which should make it possible to weave the fibers into a flexible and conformal mesh. We believe further performance improvements are possible through optimizing the fiber design.

We recommend the following next steps for advancing the fiber fuel cell technology:

- Optimize electro-plating process for fabricating electrodes on PET shrink tubing
- Develop a co extrusion fabrication process for making large quantities of fiber sufficient for woven patches/garments of desired power/energy
- Develop a power management module including energy storage to interface with the fiber fuel cell and provide pulse and steady state power capability and remaining capacity information
- Demonstrate a complete power solution by integrating the fiber fuel cell with a power management module

6.0 Bibliography

[1] Linden, D. and Reddy, T., [Handbook of Batteries], McGraw-Hill, New York, 1.12-1.13 (2002).
[2] Chiou, J and Paul, D., "Gas Permeation in Dry Nafion Membrane," Ind. Eng. Chem. Res. 27, 2161-2164 (1988).
[3] Xueping, Gan "Electroless copper plating on PET fabrics using hypophosphite as reducing agent." Surface & Coating Technology vol. 201, 7018-7023 (2007).
[4] http://www.dod.mil/ddre/prize/Winners.html
[5] Small Fuel Cells 2009 Conference Documentation
[6] Mallory, Glenn O. Hajdu, Juan B. *Electroless Plating: Fundamentals and Applications.* American Electroplaters and Surface Finishers Society. Orlando, Florida. 1990.

7.0 Acknowledgements

This material is based upon work supported by the U.S. Army Research Office and DARPA MTO under Contract No. W911NF-10-C-0007.

8.0 Appendices

Summary of Electro-less Copper Plating Experiments

Introduction

The objective of these experiments was to deposit a thin layer of gold onto a PET substrate. The proposed solution was to plate a thin seed layer of copper using electro-less plating methods, and then finishing with a layer of gold using electroplating techniques. The focus of this report will be the processes used and results obtained in the electro-less copper plating experiments.

Experimental Setup and Procedure

The proposed cylindrical chemical based fiber fuel cells to be prototyped and evaluated, require both a cathode and an anode to successfully deliver the generated power. In the initial design, very thin heat shrink tubing made of PET which is plated with a small amount of gold will serve as the electrical connections. Due to the nature of the anode and cathode function and their orientation in the overall design, the anode and cathode must be made slightly differently. The anode must have the deposited gold located only along the outside of the tubing walls, and the cathode must have the deposited gold only on the inside of the tubing walls. Due to the aforementioned requirement, some commonly used metal deposition techniques cannot be used. Included in these techniques are vapor deposition and other evaporative methods because they are not capable of evenly plating the inner walls of a tube. This inner wall constraint requires that a liquid immersion plating method be used. The most common immersion plating method is electroplating. Electroplating is a solution based plating method and is capable of plating many types of metals onto conductive substrates. The catalyst behind activating electroplating is electrical current, which is to say that a current must be passed through the electroplating solution and the conductive substrate in order for the metal deposition to occur. Since the heat shrink PET tubing to be used in the fiber fuel cell is non-conductive, electroplating cannot be used to directly plate onto the substrate.

Another immersion based metal plating technique called electroless plating does not require any electrical connection between the solution and the part to be plated. The activating energy behind electroless plating is a combination of chemical reactions and heat. This means that nonconductive parts like plastic, or in this case heat shrink PET tubing, can be metalized. After a literature review, it was decided that the goal would be to deposit a seed-layer of copper using electroless plating onto the PET tubing, and then finish the plating process by electroplating gold onto the part using a commercially available solution. A publication that described a process for electroless plating onto planar sheets of PET tubing was used as a reference and starting point to the chemical process for our experiments. The publication, entitled “Electroless Copper Plating on PET Fabrics using Hypophosphite as a Reducing Agent” by Gan et. al. describes in detail the steps and results of electrolessly plating copper onto fabric sheets of PET. The same chemicals used in this publication were purchased and prepared for the initial trials.

The reference publication implements an 11 step process for electroless copper plating. These steps include scouring, rinsing, etching, rinsing, sensitization, rinsing, activation, electroless copper plating, rinsing, and finally drying. Scouring is a pretreatment step which is designed to clean the part, and consists of 10 g/l NaOH solution at 70 ˚C for three minutes. All rinsing steps, except that before the electroless copper plating, consist of a short rinse with distilled water. Etching is a necessary step in plating plastics, as it breaks down the surface allowing for a greater surface area and improved adhesion. The publication’s etching step consists of 15 g/l

$KMnO_4$ and 40 ml/l H_2SO_4 at room temperature for three minutes. Sensitization in this case is a step which is a precursor to the activator but serves a similar purpose and is composed of 10 g/l $SnCl_2$ and 40 ml/l 38% HCl at 30 ˚C for three minutes. Activation baths in electroless plating are very important to successful adhesion. The activation bath provides many metal activation sites which are required for copper deposition. In this case palladium is the activator, with the activation bath containing 0.5 g/l $PdCl_2$ and 20 ml/l 38% HCl at 40 ˚C for five minutes. After the activation, the part is to be rinsed in a large volume of DI water for more than five minutes in order to prevent contamination of the electroless copper bath. The electroless copper plating bath is composed of 0.032 M copper sulfate ($CuSO_4$), 0.0019 to 0.0076 M nickel sulfate ($NiSO_4$), 0.283 M sodium hypophosphite ($NaPO_2H_2$), 0.071 M sodium citrate ($NaC_6H_5O_7$), 0.493 M boric acid (H_3BO_3), and 0 to 6 ppm potassium ferrocyanide ($K_4Fe(CN)_6$). All plating experiments conducted in the publication were for 10 minutes at temperatures ranging from 60 to 75 ˚C and pH ranging from 8.5 to 10.5. NaOH or H_2SO_4 was used to adjust the pH to the desired value. Finally, after the electroless copper bath, the part is rinsed and dried in an oven at 55˚C. [1]

As a jumping off point the bath compositions and operating conditions were mimicked exactly during the first experiment. Four hot plates with thermocouples were used to control the individual bath temperatures. Deionized water was used to prepare all bath solutions. pH measurements were taken with a VWR pH meter, and chemical weight measurements were taken with one of two digital readout scales accurate to the ten-thousandths or thousandths of a gram. Beakers of various sizes were used to contain the separate baths. After use of the baths, the chemicals were released down the sink drain and a log of the amount of chemicals released was kept for the records.

Results and Discussion

For ease of reporting, the baths used in experimenting will be referred to as the following: the scouring bath will be referred to as Bath 1, the etching bath as Bath 2, the sensitization bath as Bath 3, the activation bath as Bath 4, and the electroless copper plating bath as Bath 5. As previously mentioned the first plating experiment was conducted following the same procedure as recommended in Gan et. al. During the experiment Bath 3, the sensitization bath, was accidently skipped and therefore was not properly implemented. For every experiment the bath compositions, operating conditions, and substrate information was recorded in a table format. The tables below describe the working conditions for the first plating experiment. Not all plating experiment tables will be included directly in this report, for any additional experimental data please see the appendix.

Table 1: Bath Compositions for Plating #1

Bath Compositions

	Chemical	Amount (g, ml)	Concentration	
Bath 1	NaOH	1.0499	10	g/l
Bath 2	$KMnO_4$	2.2568	15	g/l
	H_2SO_4	6	40	ml/l
Bath 3	$SnCl_2$	2.1186	10	g/l
	HCl	8	40	ml/l
Bath 4	$PdCl_2$	0.0522	0.5	g/l
	HCl	1.8	20	ml/l
Bath 5	$CuSO_4$	1.0114	0.032	M
	$NiSO_4$	0.2748	0.0052	M

$NaPO_2H_2$	6.0624	0.2860	M
$NaC_6H_5O_7$	4.1531	0.0141	M
H_3BO_3	6.1624	0.4981	M
$K_4Fe(CN)_6$	0	0	ppm
NaOH	1.2458	6.229	g/l

Table 2: Operating Conditions for Plating #1

Operating Conditions

	Temp (˚C)	Time (min)	Other
Bath 1	70	3	
Bath 2	RT	3	
Bath 3	N/A	N/A	
Bath 4	30	4.25	
Bath 5	60	20	pH=8.6

Table 3: Substrate Information for Plating #1

Substrate Information

Length (cm)	Weight Before (g)	Weight After (g)
5	0.0740	0.0742

The first noticeable observation as a result of the first experiment was that the PET tubing shrank due to the bath's operating temperatures. It was observed that the piece shrank during Bath 1 immersion at a temperature of 70 ˚C, but was indeterminable whether or not Bath 5 caused any shrinkage. In terms of deposition, the plating resulted in a light yellow to gold colored very spotty deposition. There was little to no weight change during the plating and it is unsure whether or not the yellowish color is indeed actually copper. A digital multimeter was used to measure the resistance across several parts of the tubing; no resistance was successfully measured across the part. Below is a picture of the resulting PET piece after plating was finished. Not all substrates will be directly pictured in this report, for a full set of substrate pictures please refer to the appendix.

Figure 2: Photograph of PET tubing after Plating #1

At this point the cause of poor plating results is unknown, but it was known that the temperature of Bath 1 was causing shrinkage, so the temperature of Bath 1 was reduced while using the same baths as plating #1. The Bath 1 temperature was reduced from 70 ˚C to 50 ˚C. The part did not shrink in Bath 1 at this temperature. All baths were properly used in this case, and no baths were skipped. However, Bath 5, at 60 ˚C, did cause slight shrinkage in the part. The shrinkage was less substantial as during plate #1 but was still noticeable. There was much less colored deposition visible on the part compared to part #1 but some yellow colored deposits could be seen. To determine repeatability of this plating, the experiment was repeated again with another substrate with similar results. The picture below shows substrate #2 after plating.

Figure 3: Picture of Substrate #2 after Plating

The publication by Gan et. al. explains the experimental relationship between several variables and deposition rate and deposition quality. All of these variables should be tested in this experimental setup. The publication suggests that deposition rate increases as Bath 5

temperature, pH, and nickel ion concentration increases. From Gan's experimental results, temperature has a high dependence on deposition rate than pH, and the plating deposition drops off at around 60 ˚C [1]. Due to this temperature dependence, the Bath 5 temperature for the fourth plating experiment was increased to 70 ˚C. In an attempt to alleviate shrinkage of the tubing during exposure to these temperatures, the part was pre-shrunk at a higher temperature, around 100 – 120 ˚C. By pre-shrinking the PET tubing before plating, the shrinkage during plating was successfully eliminated. The deposition was once again very spotty and lightly colored yellow. The resistance of this part could not be measured, and the overall deposition was fairly poor.

The role of potassium ferrocyanide in the electroless copper plating bath is to improve the surface smoothness of the copper deposition. The publication shows that the copper deposition smoothness is improved when potassium ferrocyanide is added in concentrations ranging from 2 – 6 ppm. However, adding potassium ferrocyanide reduces the deposition rate exponentially. [1] For the fifth plating, a small amount of potassium ferrocyanide was added to the previous Bath 5 composition. Only 0.0035g was added to Bath 5, even though this is a small amount it is still well above 6 ppm concentration suggested in the publication. [1] The result of the plating was no deposition whatsoever; this is most likely a result of too much potassium ferrocyanide added to Bath 5 such that the deposition rate decreased to zero. To verify this, another plating experiment was conducted with slightly less potassium ferrocyanide, yet still above the 6 ppm level. Once again the result was no deposition onto the part. Since the potassium ferrocyanide is nearly impossible to measure at such a low concentration its usefulness in these experiments is limited, and would no longer be used in further trials.

In order to eliminate another lurking variable in these experiments, two different substrates were tested to ensure that the PET heat shrink tubing is not the reason for poor plating results. The first piece tested was a planar sheet of PET. Using the same processes as the heat shrink tubing, similar results were obtained, little to no deposition. Secondly, a cylindrical piece of delrin was plated. The piece of delrin did have some yellow-orange matte colored deposits on its surface, but the adhesion was very poor, being simply wiped off with a dry cloth. The results of these two tests help show that the poor plating depositions are not the result of the PET heat shrink tubing. Another repeatability test was conducted by plating a piece of PET tubing using the same baths at the previous trials with once again no deposition on the part.

After struggling with these initial experiments, a second literature search was conducted to learn more about electroless plating on plastics. Another strong resource for information on electroless plating was found and its ideas were applied to these experiments. The textbook called "Electroless Plating: Fundamentals and Applications" provided a somewhat detailed explanation of the fundamentals of electroless plating. In Chapter 14, *Plating on Plastics*, the common steps of electroless plating are described. The first piece of valuable information noted is the standard compositions of the activation baths. The textbook explains that previous activation processes commonly included a two bath process, and it was noted that this two bath activation process (sensitization and activation) was the same process as that being used in these experiments. The book goes on to explain that more recent activation baths consist only of a one step process that is essentially comprised of the two previous baths combined. This information was the driver behind the next set of experiments, the components of Bath 3 and Bath 4 were combined, and the concentrations were adjusted according to the textbook. [2] The table below depicts the bath compositions for plating #10.

Table 4: Bath Compositions for Plating #10

Bath Compositions

	Chemical	Amount (g, ml)	Concentration	
Bath 1	NaOH	0.916	10	g/l
Bath 2	$KMnO_4$	2.4361	15	g/l
	H_2SO_4	6	40	ml/l

Bath 3-4	$SnCl_2$	1.2256	6.128	g/l
	HCl	8	40	ml/l
	$PdCl_2$	0.0226	0.113	g/l
Bath 5	$CuSO_4$	1.0467	0.032	M
	$NiSO_4$	0.3765	0.0072	M
	$NaPO_2H_2$	6.1451	0.2899	M
	$NaC_6H_5O_7$	4.3421	0.0148	M
	H_3BO_3	6.0269	0.4871	M
	$K_4Fe(CN)_6$	0	0	ppm
	NaOH	1.2452	6.226	g/l

The result of this new plating experiment with the combined activation bath was promising. After taking the part out of the electroless copper bath the part was evenly coated with a nice layer of dark orange copper colored material. However, adhesion was still an issue because most of the copper was flaked off with a water and acetone rinse. After rinsing and drying the part, a digital multimeter was used to measure the resistance across the substrate where the orange color still remained. The multimeter was able to successfully measure a resistance across the piece, indicating that the orange colored deposition is indeed copper. The following picture shows the part (Substrate #10) after this plating experiment.

Figure 4: Substrate #10 after Plating

In order to attempt to alleviate the adhesion issues, the next plating experiment was conducted using the same baths, but the immersion time in Bath 5 was increased from 10 minutes to 30 minutes. As the part was immersed in Bath 5 it was visibly noticeable that more copper was being deposited onto the part, but as time went on the copper deposits were starting to visibly flake onto the part and eventually started to precipitate right out of the bath and sink to the bottom of the beaker. The copper deposits on the part appeared to have a stronger metallic finish at 30 minutes plating time compared to the matte finish at 10 minutes. When the part was rinsed off with water and acetone the copper once again flaked off relatively easily. This indicated that there are still adhesion issues. Another experiment was tested in which Bath 5 was made to operate as an electroless nickel bath by replacing all the copper sulfate by additional nickel sulfate. This experiment resulted in no deposition on the part. The picture below depicts substrate #11, the part which was exposed to the electroless copper bath for 30 minutes.

Figure 5: Substrate #11 after Plating for 30 Minutes

In the next experiment conducted, the hydrochloric acid concentration in the activation bath was doubled in an attempt to improve adhesion. In this case the part was not rinsed after plating and allowed to air dry. The result was fairly strong copper plating similar to plating #10 but less spotty, the part is pictured below.

Figure 6: Substrate #13 after Plating

The textbook “Electroless Plating: Fundamentals and Applications” was once again referenced in order to find a solution for the adhesion issues. It was found that the recommended sulfuric acid concentration in etching baths was considerably higher than the sulfuric acid concentration being previously used. In the following experiment, the sulfuric acid concentration was increased to 133 ml/l from 40 ml/l and the bath was set at 60 ˚C instead of room temperature. Adhesion was not significantly improved by the increase. An additional 20 ml of sulfuric acid was added to the etching bath and adhesion was improved slightly, but was still far from satisfactory. Pictured below is Substrate #15 after plating using a high concentration sulfuric acid etching bath.

Figure 7: Substrate #15

Finally as an additional attempt to improve adhesion the outer surface of a piece of PET tubing was roughed by sanding the piece with 600 particles per square inch sand paper. This

experiment did result in much better adhesion indicating that the PET's surface morphology causes a very difficult to plate environment. The part also had black spots over the surface; the cause of these spots is unknown. The final substrate which was prepped by sanding the surface is pictured below.

Figure 8: Substrate #16

Conclusion

Although an acceptable solution was ultimately not obtained, significant progress was made towards finding a solution to electrolessly plating copper onto PET heat shrink tubing. A one bath activation process works significantly better than a two bath activation process. Adhesion to the PET was the biggest hurdle which was never overcame. Increasing the sulfuric acid concentration in the etching bath does not significantly improve adhesion. Roughing the surface of the tubing does increase surface adhesion. With some more tweaking and experimentation it may be possible to find a suitable solution for this difficult to plate substrate.

Plate #1

Description: This plate was the first trial of many in electroless copper plating onto PET heat shrink tubing. Bath 3 was accidentally skipped during the process. The part shrank due to the bath temperatures. An un-uniform yellowish gold very thin deposition can be seen on the surface. This may or may not have been copper, the conductivity cannot be measured.

Bath Compositions

	Chemical	Amount (g, ml)	Concentration	
Bath 1	NaOH	1.0499	10	g/l
Bath 2	$KMnO_4$	2.2568	15	g/l
	H_2SO_4	6	40	ml/l
Bath 3	$SnCl_2$	2.1186	10	g/l
	HCl	8	40	ml/l
Bath 4	$PdCl_2$	0.0522	0.5	g/l
	HCl	1.8	20	ml/l
Bath 5	$CuSO_4$	1.0114	0.032	M
	$NiSO_4$	0.2748	0.0052	M
	$NaPO_2H_2$	6.0624	0.2860	M
	$NaC_6H_5O_7$	4.1531	0.0141	M
	H_3BO_3	6.1624	0.4981	M
	$K_4Fe(CN)_6$	0	0	ppm
	NaOH	1.2458	6.229	g/l

Operating Conditions

	Temp (˚C)	Time (min)	Other
Bath 1	70	3	
Bath 2	RT	3	
Bath 3	N/A	N/A	
Bath 4	30	4.25	

Bath 5	60	20	pH=8.6

Substrate Information

Length (cm)	Weight Before (g)	Weight After (g)
5	0.0740	0.0742

Plate #2

Description: In this trial the Bath 1 temp was reduced to 50 C to attempt to eliminate shrinkage. The part did not shrink in Bath 1, but did shrink in Bath 5. A similar yellow colored deposition can be seen, but is in a much smaller amount than plate #1.

Bath Compositions

	Chemical	Amount (g, ml)	Concentration	
Bath 1	NaOH	1.0499	10	g/l
Bath 2	$KMnO_4$	2.2568	15	g/l
	H_2SO_4	6	40	ml/l
Bath 3	$SnCl_2$	2.1186	10	g/l
	HCl	8	40	ml/l
Bath 4	$PdCl_2$	0.0522	0.5	g/l
	HCl	1.8	20	ml/l
Bath 5	$CuSO_4$	1.0114	0.032	M
	$NiSO_4$	0.2748	0.0052	M
	$NaPO_2H_2$	6.0624	0.2860	M
	$NaC_6H_5O_7$	4.1531	0.0141	M
	H_3BO_3	6.1624	0.4981	M
	$K_4Fe(CN)_6$	0	0	ppm
	NaOH	1.2458	6.229	g/l

Operating Conditions

	Temp (˚C)	Time (min)	Other
Bath 1	50	3	
Bath 2	RT	3	
Bath 3	30	3	
Bath 4	40	5	
Bath 5	60	15	pH=8.6

Substrate Information

Length (cm)	Weight Before (g)	Weight After (g)
5	0.0744	0.0745

Plate #3

Description: For this plating, the temperature of Bath 5 was reduced to 50 C. Little to no deposition was achieved, most likely due to the low electroless copper bath temp.

No picture available.

Bath Compositions

	Chemical	Amount (g, ml)	Concentration	
Bath 1	NaOH	1.0499	10	g/l
Bath 2	$KMnO_4$	2.2568	15	g/l
	H_2SO_4	6	40	ml/l
Bath 3	$SnCl_2$	2.1186	10	g/l
	HCl	8	40	ml/l
Bath 4	$PdCl_2$	0.0522	0.5	g/l
	HCl	1.8	20	ml/l
Bath 5	$CuSO_4$	1.0114	0.032	M
	$NiSO_4$	0.2748	0.0052	M
	$NaPO_2H_2$	6.0624	0.2860	M
	$NaC_6H_5O_7$	4.1531	0.0141	M
	H_3BO_3	6.1624	0.4981	M
	$K_4Fe(CN)_6$	0	0	ppm
	NaOH	1.2458	6.229	g/l

Operating Conditions

	Temp (˚C)	Time (min)	Other
Bath 1	50	3	
Bath 2	RT	3	

Bath 3	30	3	
Bath 4	40	5	
Bath 5	50	15	pH=8.68

Substrate Information

Length (cm)	Weight Before (g)	Weight After (g)
5	0.0319	

Plate #4

Description: In this plating the part was pre-shrunk in an oven before exposed to any chemical baths to attempt to eliminate shrinkage due to high bath temperatures. The final part had no shrinkage even at a Bath 5 temperature of 70 C. However, there is once again a very little yellowish colored thin and spotty deposition.

Bath Compositions

	Chemical	Amount (g, ml)	Concentration	
Bath 1	NaOH	0.9074	10	g/l
Bath 2	$KMnO_4$	2.3495	15	g/l
	H_2SO_4	6	40	ml/l
Bath 3	$SnCl_2$	2.0832	10	g/l
	HCl	8	40	ml/l
Bath 4	$PdCl_2$	0.0725	0.5	g/l
	HCl	1.8	20	ml/l
Bath 5	$CuSO_4$	1.0452	0.032	M
	$NiSO_4$	0.3859	0.0073	M
	$NaPO_2H_2$	5.9861	0.2824	M
	$NaC_6H_5O_7$	4.1827	0.0142	M
	H_3BO_3	6.1624	0.4981	M
	$K_4Fe(CN)_6$	0	0	ppm
	NaOH	1.3052	6.526	g/l

Operating Conditions

	Temp (˚C)	Time (min)	Other
Bath 1	50	3	
Bath 2	RT	3	
Bath 3	30	3	
Bath 4	40	5	
Bath 5	70	15	pH=8.6

Substrate Information

Length (cm)	Weight Before (g)	Weight After (g)
4.8	0.0215	0.0215

Plate #5

Description: During this experiment, the same baths as plate #4 were used except some potassium ferrocyanide was added to Bath 5. Even though very little was added, it is still well above the recommended limit. There was no deposition at all onto the substrate. This is most likely due to too much potassium ferrocyanide.

Bath Compositions

	Chemical	Amount (g, ml)	Concentration	
Bath 1	NaOH	0.9074	10	g/l
Bath 2	$KMnO_4$	2.3495	15	g/l
	H_2SO_4	6	40	ml/l
Bath 3	$SnCl_2$	2.0832	10	g/l
	HCl	8	40	ml/l
Bath 4	$PdCl_2$	0.0725	0.5	g/l
	HCl	1.8	20	ml/l
Bath 5	$CuSO_4$	1.0452	0.032	M
	$NiSO_4$	0.3859	0.0073	M
	$NaPO_2H_2$	5.9861	0.2824	M
	$NaC_6H_5O_7$	4.1827	0.0142	M
	H_3BO_3	6.1624	0.4981	M
	$K_4Fe(CN)_6$	0.0035	700	ppm

NaOH	1.3052	6.526	g/l

Operating Conditions

	Temp (˚C)	Time (min)	Other
Bath 1	50	3	
Bath 2	RT	3	
Bath 3	30	3	
Bath 4	40	5	
Bath 5	70	15	pH=8.6

Substrate Information

Length (cm)	Weight Before (g)	Weight After (g)
5.2	0.0236	

Plate #6

Description: New baths were mixed for this experiment, and once again potassium ferrocyanide was used. The pH of Bath 5 was raised more than previous baths. There was once again little to no deposition on the substrate, this could again be due to a high amount of potassium ferrocyanide.

Bath Compositions

	Chemical	Amount (g, ml)	Concentration	
Bath 1	NaOH	0.9037	10	g/l
Bath 2	$KMnO_4$	2.3086	15	g/l
	H_2SO_4	6	40	ml/l
Bath 3	$SnCl_2$	1.9472	10	g/l
	HCl	8	40	ml/l
Bath 4	$PdCl_2$	0.0521	0.5	g/l
	HCl	1.8	20	ml/l
Bath 5	$CuSO_4$	1.0467	0.032	M
	$NiSO_4$	0.3765	0.0072	M
	$NaPO_2H_2$	6.1451	0.2899	M
	$NaC_6H_5O_7$	4.3421	0.0148	M
	H_3BO_3	6.0269	0.4871	M

$K_4Fe(CN)_6$	0.003	600	ppm
NaOH	2.1276	10.638	g/l

Operating Conditions

	Temp (˚C)	Time (min)	Other
Bath 1	50	3	
Bath 2	RT	3	
Bath 3	30	3	
Bath 4	40	5	
Bath 5	70	10	pH=9.7

Substrate Information

Length (cm)	Weight Before (g)	Weight After (g)
5.5	0.0250	0.0263

Plate #7

Description: This attempt was conducted on a piece of planar PET to see if the heat shrink tubing is a cause for deposition problems. The planar PET piece also had no copper deposition.

No picture available

Bath Compositions

	Chemical	Amount (g, ml)	Concentration	
Bath 1	NaOH	0.9037	10	g/l
Bath 2	$KMnO_4$	2.3086	15	g/l
	H_2SO_4	6	40	ml/l
Bath 3	$SnCl_2$	1.9472	10	g/l
	HCl	8	40	ml/l
Bath 4	$PdCl_2$	0.0521	0.5	g/l
	HCl	1.8	20	ml/l
Bath 5	$CuSO_4$	1.0467	0.032	M
	$NiSO_4$	0.3765	0.0072	M
	$NaPO_2H_2$	6.1451	0.2899	M
	$NaC_6H_5O_7$	4.3421	0.0148	M
	H_3BO_3	6.0269	0.4871	M
	$K_4Fe(CN)_6$	0	0	ppm
	NaOH	2.1276	10.638	g/l

Operating Conditions

	Temp (˚C)	Time (min)	Other
Bath 1	50	3	

Bath 2	RT	3	
Bath 3	30	3	
Bath 4	40	5	
Bath 5	70	10	pH=9.7

Substrate Information

Length (cm)	Weight Before (g)	Weight After (g)
8.7x2	0.1325	0.1214

Plate #8

Description: A piece of delrin was used as a substrate. A matte orange colored spotty deposition was achieved, but was easily wiped completely off.

No Picture Available

Bath Compositions

	Chemical	Amount (g, ml)	Concentration	
Bath 1	NaOH	0.9037	10	g/l
Bath 2	$KMnO_4$	2.3086	15	g/l
	H_2SO_4	6	40	ml/l
Bath 3	$SnCl_2$	1.9472	10	g/l
	HCl	8	40	ml/l
Bath 4	$PdCl_2$	0.0521	0.5	g/l
	HCl	1.8	20	ml/l
Bath 5	$CuSO_4$	1.0467	0.032	M
	$NiSO_4$	0.3765	0.0072	M
	$NaPO_2H_2$	6.1451	0.2899	M
	$NaC_6H_5O_7$	4.3421	0.0148	M
	H_3BO_3	6.0269	0.4871	M
	$K_4Fe(CN)_6$	0	0	ppm
	NaOH	2.1276	10.638	g/l

Operating Conditions

	Temp (˚C)	Time (min)	Other
Bath 1	50	3	
Bath 2	RT	3	
Bath 3	30	3	
Bath 4	40	5	
Bath 5	70	10	pH=9.7

Substrate Information

Length (cm)	Weight Before (g)	Weight After (g)
7.8x0.4	1.7939	1.7911

Plate #9
Description: The procedure for plate #6 was repeated and once again no deposition was achieved.

Bath Compositions

	Chemical	Amount (g, ml)	Concentration	
Bath 1	NaOH	0.9037	10	g/l
Bath 2	$KMnO_4$	2.3086	15	g/l
	H_2SO_4	6	40	ml/l
Bath 3	$SnCl_2$	1.9472	10	g/l
	HCl	8	40	ml/l
Bath 4	$PdCl_2$	0.0521	0.5	g/l
	HCl	1.8	20	ml/l
Bath 5	$CuSO_4$	1.0467	0.032	M
	$NiSO_4$	0.3765	0.0072	M
	$NaPO_2H_2$	6.1451	0.2899	M
	$NaC_6H_5O_7$	4.3421	0.0148	M
	H_3BO_3	6.0269	0.4871	M
	$K_4Fe(CN)_6$	0	0	ppm
	NaOH	2.1276	10.638	g/l

Operating Conditions

	Temp (˚C)	Time (min)	Other
Bath 1	50	3	
Bath 2	RT	3	
Bath 3	30	3	
Bath 4	40	5	

Bath 5	70	10	pH=9.7

Substrate Information

Length (cm)	Weight Before (g)	Weight After (g)
5.5	0.0259	

Plate #10

Description: In this experiment, and the following experiments, the overall bath arrangement was changed. The original Bath 3 and Bath 4 were essentially combined, with a slight change in concentrations; this bath is referred to as Bath 3-4. This resulted in an orange, copper colored but relatively spotty deposition. The adhesion of the deposition is fairly poor.

Bath Compositions

	Chemical	Amount (g, ml)	Concentration	
Bath 1	NaOH	0.916	10	g/l
Bath 2	$KMnO_4$	2.4361	15	g/l
	H_2SO_4	6	40	ml/l
Bath 3-4	$SnCl_2$	1.2256	6.128	g/l
	HCl	8	40	ml/l
	$PdCl_2$	0.0226	0.113	g/l
Bath 5	$CuSO_4$	1.0467	0.032	M
	$NiSO_4$	0.3765	0.0072	M
	$NaPO_2H_2$	6.1451	0.2899	M
	$NaC_6H_5O_7$	4.3421	0.0148	M
	H_3BO_3	6.0269	0.4871	M
	$K_4Fe(CN)_6$	0	0	ppm
	NaOH	1.2452	6.226	g/l

Operating Conditions

	Temp (˚C)	Time (min)	Other
Bath 1	70	3	
Bath 2	RT	3	

Bath 3-4	35	5	
Bath 5	70	10	pH=9.09

Substrate Information

Length (cm)	Weight Before (g)	Weight After (g)
	0.0263	0.0286

Plate #11

Description: The steps in this plating were similar to plate #10 except that the part was immersed in the electroless copper bath for 30 minutes. Bath 5 was clearly deposition more copper onto the substrate, but adhesion was still poor. Near the end of the deposition the copper was visibly precipitation out of the solution and dropping to the bottom of the beaker. After plating, the majority of the copper was easily rinsed off, leaving a very spotty but metallic copper deposition.

Bath Compositions

	Chemical	Amount (g, ml)	Concentration	
Bath 1	NaOH	0.972	10	g/l
Bath 2	$KMnO_4$	2.245	15	g/l
	H_2SO_4	6	40	ml/l
Bath 3-4	$SnCl_2$	1.254	6.27	g/l
	HCl	8	40	ml/l
	$PdCl_2$	0.025	0.125	g/l
Bath 5	$CuSO_4$	1.001	0.032	M
	$NiSO_4$	0.327	0.0062	M
	$NaPO_2H_2$	6.032	0.2846	M
	$NaC_6H_5O_7$	4.165	0.0142	M
	H_3BO_3	6.059	0.4897	M
	$K_4Fe(CN)_6$	0	0	ppm
	NaOH	1.25	6.25	g/l

Operating Conditions

	Temp (˚C)	Time (min)	Other
Bath 1	70	3	
Bath 2	RT	3	

Bath 3-4	35	5	
Bath 5	70	30	pH=8.87

Substrate Information

Length (cm)	Weight Before (g)	Weight After (g)
	0.027	0.026

Plate #12

Description: In this experiment a purely nickel electroless bath was attempted by eliminating the copper sulfate and adding more nickel sulfate. The result was no deposition onto the substrate.

Bath Compositions

	Chemical	Amount (g, ml)	Concentration	
Bath 1	NaOH	0.972	10	g/l
Bath 2	$KMnO_4$	2.245	15	g/l
	H_2SO_4	6	40	ml/l
Bath 3-4	$SnCl_2$	1.254	6.27	g/l
	HCl	8	40	ml/l
	$PdCl_2$	0.025	0.125	g/l
Bath 5	$CuSO_4$	0	0	M
	$NiSO_4$	1.611	0.0306	M
	$NaPO_2H_2$	6.042	0.2850	M
	$NaC_6H_5O_7$	4.159	0.0141	M
	H_3BO_3	6.005	0.4854	M
	$K_4Fe(CN)_6$	0	0	ppm
	NaOH	1.113	5.565	g/l

Operating Conditions

	Temp (˚C)	Time (min)	Other
Bath 1	70	3	
Bath 2	RT	3	

Bath 3-4	35	5	
Bath 5	70	10	pH=8.98

Substrate Information

Length (cm)	Weight Before (g)	Weight After (g)
	0.026	0.026

Plate #13

Description: Additional HCl was added to Bath 3-4. Result was medium spotty matte copper colored deposition similar to that of plate #10.

Bath Compositions

	Chemical	Amount (g, ml)	Concentration	
Bath 1	NaOH	0.972	10	g/l
Bath 2	$KMnO_4$	2.245	15	g/l
	H_2SO_4	6	40	ml/l
Bath 3-4	$SnCl_2$	1.254	6.27	g/l
	HCl	16	80	ml/l
	$PdCl_2$	0.025	0.125	g/l
Bath 5	$CuSO_4$	1.001	0.032	M
	$NiSO_4$	0.327	0.0062	M
	$NaPO_2H_2$	6.032	0.2846	M
	$NaC_6H_5O_7$	4.165	0.0142	M
	H_3BO_3	6.059	0.4897	M
	$K_4Fe(CN)_6$	0	0	ppm
	NaOH	1.25	6.25	g/l

Operating Conditions

	Temp (˚C)	Time (min)	Other
Bath 1	70	3	
Bath 2	RT	3	

Bath 3-4	35	5	
Bath 5	70	15	pH=8.98

Substrate Information

Length (cm)	Weight Before (g)	Weight After (g)
	0.027	

Plate #14

Description: The sulfuric acid concentration of bath 2 was increased substantially, and the bath was set at 60 C at an attempt to increase etching and adhesion. The result was a darker, more typical copper colored deposition, but adhesion was still fairly poor, with most of the deposition rinsing off with water.

Bath Compositions

	Chemical	Amount (g, ml)	Concentration	
Bath 1	NaOH	0.947	10	g/l
Bath 2	$KMnO_4$	2.358	15	g/l
	H_2SO_4	20	133	ml/l
Bath 3-4	$SnCl_2$	1.279	6.395	g/l
	HCl	8	40	ml/l
	$PdCl_2$	0.04	0.2	g/l
Bath 5	$CuSO_4$	1.004	0.032	M
	$NiSO_4$	0.322	0.0061	M
	$NaPO_2H_2$	6.023	0.2841	M
	$NaC_6H_5O_7$	4.122	0.0140	M
	H_3BO_3	5.998	0.4848	M
	$K_4Fe(CN)_6$	0	0	ppm
	NaOH	1.326	6.63	g/l

Operating Conditions

	Temp (˚C)	Time (min)	Other
Bath 1	70	3	
Bath 2	60	3	

Bath 3-4	35	5	
Bath 5	70	15	pH=8.90

Substrate Information

Length (cm)	Weight Before (g)	Weight After (g)
	0.026	0.027

Plate #15

Description: An additional 20 ml of sulfuric acid was added to bath 2 in an attempt to further increase etching and adhesion. The result was a slightly better adhering deposition, yet could still be rinsed off after rinsing. Bath 2 was in ambient conditions but was warmed due to the exothermic reaction the sulfuric acid and water was creating.

Bath Compositions

	Chemical	Amount (g, ml)	Concentration	
Bath 1	NaOH	0.947	10	g/l
Bath 2	$KMnO_4$	2.358	15	g/l
	H_2SO_4	40	266	ml/l
Bath 3-4	$SnCl_2$	1.279	6.395	g/l
	HCl	8	40	ml/l
	$PdCl_2$	0.04	0.2	g/l
Bath 5	$CuSO_4$	1.004	0.032	M
	$NiSO_4$	0.322	0.0061	M
	$NaPO_2H_2$	6.023	0.2841	M
	$NaC_6H_5O_7$	4.122	0.0140	M
	H_3BO_3	5.998	0.4848	M
	$K_4Fe(CN)_6$	0	0	ppm
	NaOH	1.326	6.63	g/l

Operating Conditions

	Temp (˚C)	Time (min)	Other
Bath 1	70	3	
Bath 2	RT*	3	Exothermic
Bath 3-4	35	5	

Bath 5	70	10	pH=8.90

Substrate Information

Length (cm)	Weight Before (g)	Weight After (g)
	0.027	0.037

Plate #16

Description: The PET substrate was sanded with 600 grit sandpaper before chemical treatment to increase surface area and roughness for better adhesion. Adhesion was increased but many small black spots are visible along the tubing's surface.

Bath Compositions

	Chemical	Amount (g, ml)	Concentration	
Bath 1	NaOH	0.9	10	g/l
Bath 2	$KMnO_4$	2.234	15	g/l
	H_2SO_4	30	200	ml/l
Bath 3-4	$SnCl_2$	1.274	6.37	g/l
	HCl	8	40	ml/l
	$PdCl_2$	0.042	0.21	g/l
Bath 5	$CuSO_4$	1.001	0.032	M
	$NiSO_4$	0.034	0.0006	M
	$NaPO_2H_2$	6.021	0.2840	M
	$NaC_6H_5O_7$	4.127	0.0140	M
	H_3BO_3	6.002	0.4851	M
	$K_4Fe(CN)_6$	0	0	ppm
	NaOH	1.285	8.86	g/l

Operating Conditions

	Temp (˚C)	Time (min)	Other
Bath 1	70	3	

Bath 2	RT*	3	Exothermic
Bath 3-4	35	5	
Bath 5	70	10	pH=8.90

Substrate Information

Length (cm)	Weight Before (g)	Weight After (g)
	0.027	